In Situ Generation of n-Type Dopants by Thermal Decarboxylation

Filip Aniés, Mohamad Nugraha, Arona Fall, Julianna Panidi, Yuxi Zhao, Patrice Vanelle, Leonidas Tsetseris, Julie Broggi Broggi, Thomas Anthopoulos, Martin Heeney

RESEARCH ARTICLE

ADVANCED FUNCTIONAL MATERIALS
www.afm-journal.de

In Situ Generation of n-Type Dopants by Thermal Decarboxylation

Filip Aniés, Mohamad I. Nugraha, Arona Fall, Julianna Panidi, Yuxi Zhao, Patrice Vanelle, Leonidas Tsetseris, Julie Broggi, Thomas D. Anthopoulos,* and Martin Heeney**

Molecular doping is a powerful and increasingly popular approach toward enhancing electronic properties of organic semiconductors (OSCs) past their intrinsic limits. The development of n-type dopants has been hampered, however, by their poor stability and high air-reactivity, a consequence of their generally electron rich nature. Here, the use of air-stable carboxylated dopant precursors is reported to overcome this challenge. Active dopants are readily generated in solution by thermal decarboxylation and applied in n-type organic field-effect transistors (OFETs). Both 1,3-dimethylimidazolium-2-carboxylate (CO_2-DMI) and novel dopant 1,3-dimethylbenzimidazolium-2-carboxylate (CO_2-DMBI) are applied to n-type OFETs employing well-known organic semiconductors (OSCs) P(NDI2OD-T2), PCBM, and O-IDTBR. Successful improvement of performance in all devices demonstrates the versatility of the dopants across a variety of OSCs. Experimental and computational studies indicate that electron transfer from the dopant to the host OSC is preceded by decarboxylation of the precursor, followed by dimerization to form the active dopant species. Transistor studies highlight CO_2-DMBI as the most effective dopant, improving electron mobility by up to one order of magnitude, while CO_2-DMI holds the advantage of commercial availability.

1. Introduction

In the past few decades, organic semiconductors (OSCs) have developed from lab curiosities to commercial applications. They have found use in technologies such as organic field-effect transistors (OFETs), organic light-emitting diodes (OLEDs), and organic photovoltaics (OPVs), among others. The use of OSCs offers several advantages compared to conventional technologies, such as more scalable manufacturing through printing and roll-to-roll methods, material customizability with respect to physical properties, and the development of flexible and transparent devices.[1–3]

Efforts toward improved and commercially competitive device performance have generally been spearheaded by research in material design, device structure, and fabrication methodologies.[4] Over the past decade, the doping of organic semiconductors has increased in popularity as a means to alter material properties and improve device performance.[5,6] Progress in this area has been particularly valuable for the development of efficient OLED devices, and the use of dopants has also led to some of the highest efficiency OPV devices reported to date.[7–10]

There have been significant advances in the development of new doping techniques for OFETs, particularly by adding dopant additives directly to the OSC layer.[11–13] The use of p-dopants has been particularly well studied, with several efficient and readily available p-dopants reported since the mid-00s,

F. Aniés, J. Panidi, M. Heeney
Department of Chemistry and Centre for Processable Electronics
Imperial College London
Molecular Sciences Research Hub
82 Wood Lane W12 0BZ, London, UK
E-mail: m.heeney@imperial.ac.uk

M. I. Nugraha, T. D. Anthopoulos, M. Heeney
KAUST Solar Center (KSC)
Physical Science and Engineering Division (PSE)
King Abdullah University of Science and Technology (KAUST)
Thuwal 23955–6900, Saudi Arabia
E-mail: thomas.anthopoulos@kaust.edu.sa

The ORCID identification number(s) for the author(s) of this article can be found under https://doi.org/10.1002/adfm.202212305.

DOI: 10.1002/adfm.202212305

M. I. Nugraha
Research Center for Advanced Materials
National Research and Innovation Agency (BRIN)
South Tangerang, Banten 15314, Indonesia

A. Fall, Y. Zhao, P. Vanelle, J. Broggi
Aix Marseille Univ
CNRS
Institut de Chimie Radicalaire ICR
Faculté de Pharmacie 13005, Marseille, France
E-mail: julie.broggi@univ-amu.fr

L. Tsetseris
Department of Physics
School of Applied Mathematical and Physical Sciences
National Technical University of Athens
GR-15780 Athens, Greece

which may be added to the OSC layer via thermal deposition, through admixing, or via post-deposition techniques.[14–18] Although n-dopants have also been investigated for many years, their transition from fundamental research to common practice has progressed more slowly than that for p-dopants.[5,11] One of the main obstacles has been the air sensitivity of n-type dopants, a consequence of their typically electron rich nature. This is particularly the case for dopants that work by the electron transfer mechanisms, in which an electron is transferred from the highest occupied molecular orbital (HOMO) of the dopant to the lowest unoccupied molecular orbital (LUMO) of the host. In order to make this energetically favorable, the dopant should have a high lying HOMO (i.e., small ionization potential), but this can lead to difficulties with synthesis, storage, and handling.[19–21]

One approach to solving the air-sensitivity issues has been the development of n-dopants that work by alternative mechanisms. For example, one of the most popular n-type dopants to date, (4-(1,3-dimethyl-2,3-dihydro-1*H*-benzoimidazol-2-yl) phenyl)dimethylamine (N-DMBI), belongs to a class of dopants that act through a doping mechanism involving hydride transfer, rather than electron transfer.[22–24] Such species are typically air stable, but can suffer from the drawback of undesired side products as a result of the hydride transfer mechanism, as well as poor predictability regarding their suitability with different OSCs.[23] An alternative strategy to address stability concerns is the design of so-called precursor-type dopants: air-stable dopant precursors that can be activated in the presence of the OSC. Examples of such dopants include dimeric species where electron transfer is coupled with the cleavage of weak C—C bonds – a mechanism that may be initiated thermally or through photoactivation.[25–30]

In our search for new precursor type dopants, we drew inspiration from the field of so-called super-electron donors, in which organometallic reductants have been replaced by fully organic reducing agents.[31–33] These are often based on highly electron rich amine substituted alkenes, which are formed by dimerization of carbene precursors. Facing similar issues with air-stability, Broggi and co-workers have pioneered the use of carboxylate protected carbene precursors, which are bench stable, but can be thermally decarboxylated in situ to form carbenes. Their subsequent dimerization generates the active reducing agent. Such species include 1,3-dimethylimidazolium-2-carboxylate (CO_2-DMI) and 1,3-dimethylbenzimidazolium-2-carboxylate (CO_2-DMBI), displaying chemical stability under ambient atmosphere over several months.[34,35] This concept has also recently been demonstrated in the context of doping by Pei and co-workers, who utilized CO_2-DMI via a post-deposition doping approach in thermoelectric devices.[36]

In this work we explore the use of air-stable carboxylate adducts as dopants for the active layer of OFET devices. We show that CO_2-DMI and the novel dopant CO_2-DMBI can be used to dope n-type OSCs through in situ thermal activation in the solution formulation, prior to coating. Furthermore, the versatility of these dopants is demonstrated through successful implementation in a variety of n-type OSCs – P(NDI2OD-T2) (also known as N2200), PCBM, and O-IDTBR (full chemical names provided in the Supporting Information) – encompassing both polymeric and small molecule species with varying energetic characteristics (**Figure 1**). We investigate the origin of the doping effect and compare electronic and morphological effects of the two dopant precursors. Our findings show that CO_2-DMBI is the more effective dopant throughout, improving electron mobility by up to one order of magnitude compared to the pristine semiconductor.

2. Results and Discussion

2.1. Optoelectronic Properties of Doped Systems

While doping mechanisms may vary, and sometimes emphasize different aspects of device physics, they generally include an alteration of the electronic properties of the host material upon charge transfer between the host and the dopant.[5,37] Several studies on doping mechanisms have established integer charge transfer, i.e., electron transfer between the dopant and the host material, as one of the main doping mechanisms, although there are variations between different doping systems.[38–42] As electron transfer in a doping context holds many similarities with redox chemistry, investigating the optoelectronic and electrochemical properties of dopant/OSC blends is a simple screen for the possibility of device doping and helps to establish the doping mechanism.

As an initial indication of relevant electron transfer processes, absorption spectra were collected for pristine and doped OSC solutions in chlorobenzene. Studying the normalized absorption spectra of P(NDI2OD-T2) solutions doped with CO_2-DMI and CO_2-DMBI shows a clear suppression and slight blue-shift of the peak ≈700 nm, with the emergence of a new peak ≈485 nm upon doping (**Figure 2**a; Figure S1, Supporting Information). This change is more prominent upon doping with a very high dopant concentration (10 wt.%), and is very similar to absorption trends observed upon electrochemical reduction of P(NDI2OD-T2), indicating the formation of a radical anionic species.[43] Similar effects have also been observed in previous studies of doping of P(NDI2OD-T2).[44–46] The effect was much more pronounced with CO_2-DMI compared to CO_2-DMBI, indicating a more reductive effect upon thermal activation of CO_2-DMI.

Normalized absorption spectra of doped PCBM solutions show a slight increase in intensity of the broad peak ≈500 nm and the sharp peak ≈430 nm, along with a lesser drop in intensity ≈315 nm (Figure 2a; Figure S2, Supporting Information). These changes are more pronounced with CO_2-DMI, which also elevates the baseline in the region above 700 nm. Similar trends have been observed in previous studies investigating n-doping of PCBM and its derivatives, once again indicating the formation of radical anions.[40,47,48]

Meanwhile, differences in absorption spectra of pure and doped O-IDTBR solutions are more subtle, with high dopant concentrations (10 wt.%) leading to a very slight blue-shift of the main peak ≈645 nm and a slight enhancement of the peak ≈405 nm. The blue shift is much more pronounced in thin films (Figure S3, Supporting Information), which is possibly an effect of changes in morphology rather than energetic properties. Once again, CO_2-DMI has a stronger effect on the absorption spectra than CO_2-DMBI. In the case of thin-film

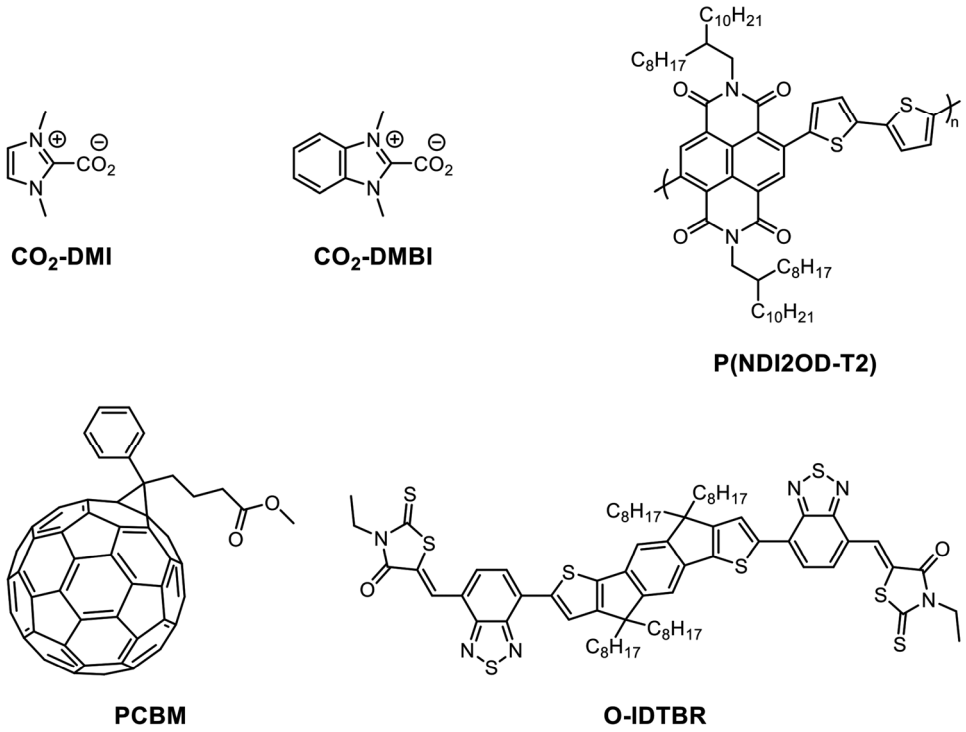

Figure 1. Molecular structures of dopants CO_2-DMI and CO_2-DMBI and investigated host OSCs.

absorption spectra of P(NDI2OD-T2) and PCBM, trends are less pronounced, and more difficult to interpret, possibly as an effect of competing morphological and energetic effects on the absorption characteristics (Figures S1, S2, Supporting Information).

To confirm the electron transfer from dopants to host materials and the formation of radical ionic species in doped thin-films, electron paramagnetic resonance (EPR) spectroscopy was conducted.[49] Figure 2b shows the normalized spectra of films of each OSC material, doped with 1 wt.% of each dopant. Sharp peaks in the region ≈3375 G (g-factor 2.000–2.005, Figure S4, Supporting Information) confirm the presence of unpaired electrons in all doped systems.[50] In contrast, EPR peaks are completely absent in pristine films in all cases, as would be expected for the neutral species. These trends align well with those typically seen in doping processes involving integer charge transfer.[49]

2.2. Dopant Activation

Previous studies on carboxylate precursors have provided insights into the activation mechanism of such species.[34,35] It is clear that the carboxylate group – that acts as a stabilizing

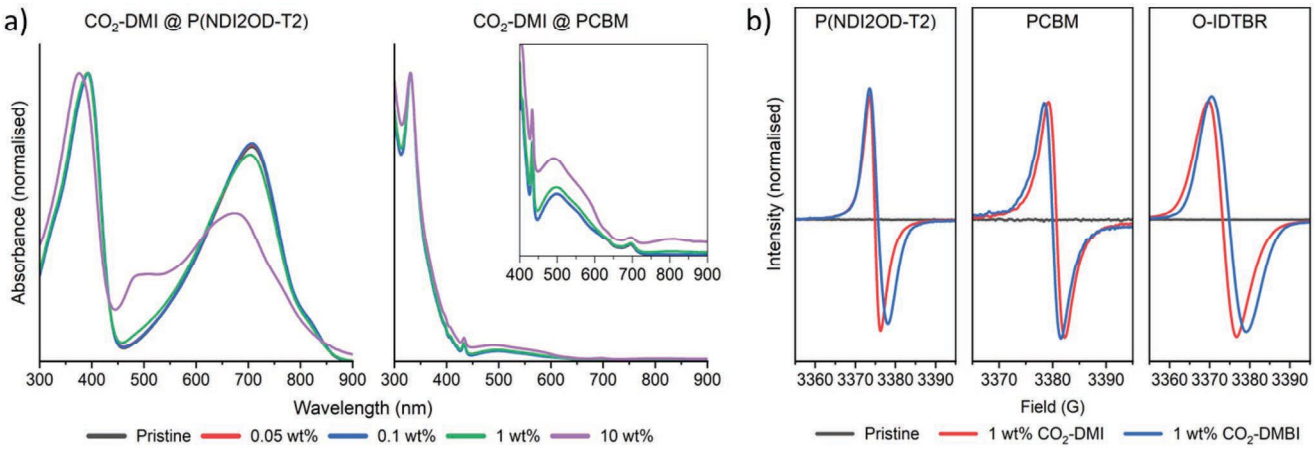

Figure 2. a) Normalized absorption spectra of P(NDI2OD-T2) and PCBM solutions doped with various amounts of CO_2-DMI in chlorobenzene. b) EPR spectra of drop-cast films of each investigated OSC doped with 1 wt.% CO_2-DMI and CO_2-DMBI.

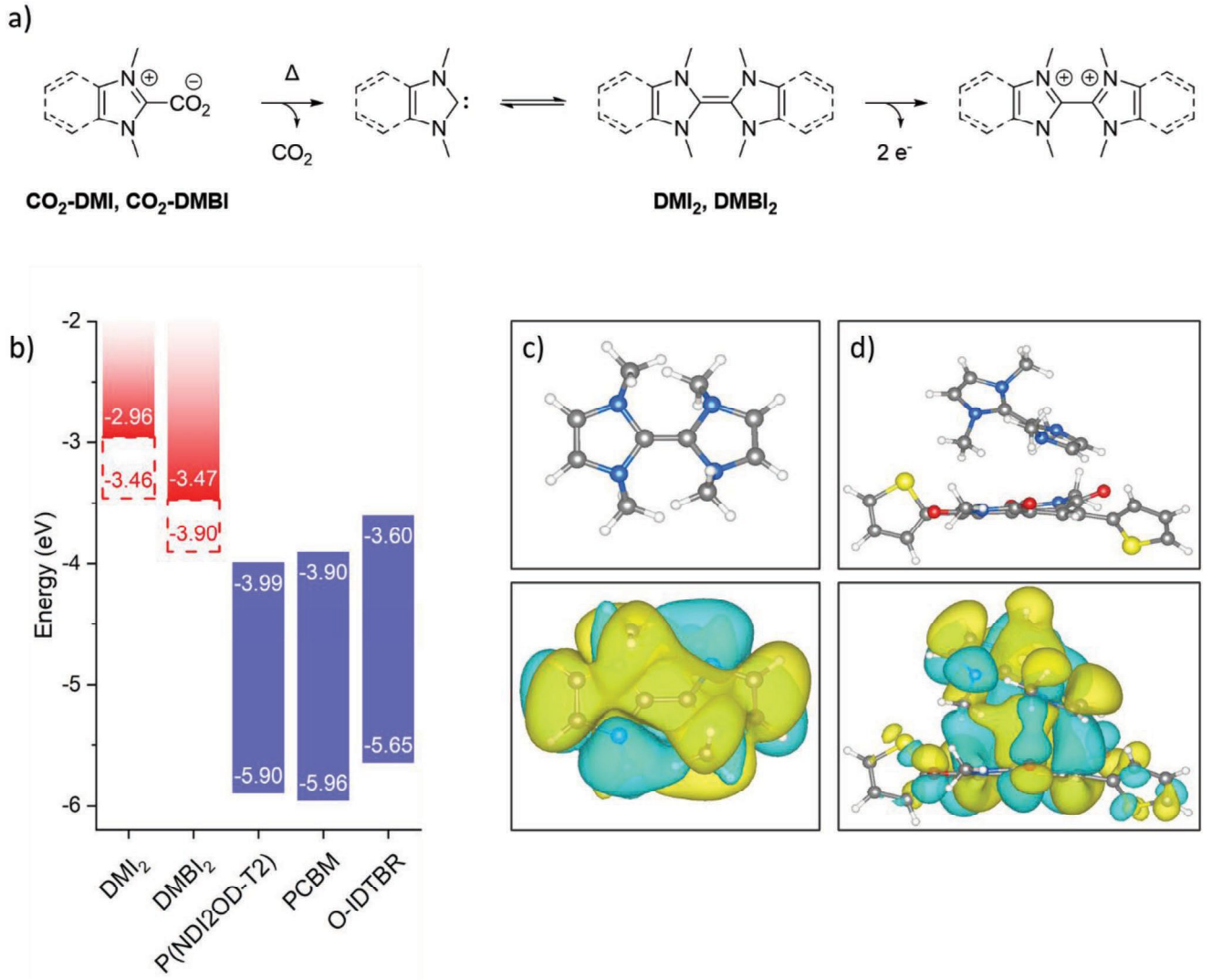

Figure 3. a) Illustration of the dopant activation process, including thermal decarboxylation, carbene dimerization, and electron donation. b) Diagram showcasing the frontier molecular orbital energy levels of active dopant dimers and OSCs. Solid red bars denote energy levels as estimated from CV of cationic dimer salts, and red dashed lines as predicted with DFT of neutral dopant dimers. c) Molecular conformation and HOMO of the DMI_2 dimer as calculated with DFT. d) Conformation and hybridized HOMO of DMI_2 physisorbed onto a P(NDI2OD-T2) monomeric unit as calculated with DFT.

group against spontaneous oxidation in air or other environments – is removed as carbon dioxide gas upon heating, leaving behind an *N*-heterocyclic carbene (NHC). In the case of CO_2-DMBI, the addition of small amounts of water, or UV radiation, has also been demonstrated to accelerate the activation.[35] NHCs are known to reversibly dimerize into their corresponding tetraazafulvalenes, in a process known as the Wanzlick equilibrium, with the position of the equilibrium determined by a variety of factors, such as *N*-substituents and the singlet-triplet energy gap.[51–55] It is typically these neutral dimeric species that act as electron donors, driven by aromatic stabilization of the oxidized products (**Figure 3**a).[33] The dimeric form of NHCs has been thoroughly studied in the context of chemical reduction, including the investigation of numerous diimidazolinylidenes and dibenzimidazolinylidene derivatives.[31–33]

Di-1,3-dimethylbenzimidazolin-2-ylidene ($DMBI_2$) has been exemplified in literature as a thermodynamically stable dimer, benefitting from a singlet-triplet energy gap lower than that of DMI_2 and little disruption of any aromatic properties after dimerization, as its aromatic character is located primarily on the fused benzene ring and may not fully extend to the 5-membered ring.[53,56] Likewise, mechanistic studies of CO_2-DMBI confirmed the formation of $DMBI_2$ upon decarboxylation: as the carboxylate adduct was heated in presence of hexachloroethane (C_2Cl_6), a dichloride salt of the dimer formed, confirming the formation of highly reductive $DMBI_2$.[35] Notably, the $DMBI_2$ dimer has a structure similar to previously reported dopant DMBI-BDZC, and to some extent tetrakis(dimethylamino)ethylene (TDAE).[57,58]

Imidazolin-2-ylidene, on the other hand, exists primarily as a monomeric carbene, with a near thermoneutral dimerization,

insufficient of overcoming the entropic loss and kinetic barriers thereof.[53,56,59] Although DMI_2 has been successfully isolated through reduction of its oxidized form, it is extremely unstable, and decomposes into the monomeric carbene within minutes.[60] Furthermore, mechanistic studies of the decarboxylation of CO_2-DMI in dimethylformamide (DMF) has suggested the formation of a formamide-derived electron donor following deprotonation of the solvent by the monomeric carbene.[34] Meanwhile, it is less certain what species would act as the active dopant in an aprotic environment in the absence of DMF.[36] To investigate this matter, we heated CO_2-DMI and C_2Cl_6 in anhydrous chlorobenzene at 80 °C for 1 h. Mass spectrometry and ^{1}H NMR spectroscopy of the resulting solids confirmed the presence of DMI_2Cl_2, suggesting that DMI_2 may be the reducing/doping species upon thermal activation of CO_2-DMI in chlorobenzene (Figures S5, S6, Supporting Information).[60] We also note that the strong nucleophilic and electron-donating ability of carbene has been observed to result in doping by nucleophilic addition to the organic semiconductor in certain cases, and we cannot rule out a similar mechanism occurring here[36,61]

To further confirm that the dimers are capable of doping OSCs we prepared chemically pure $DMBI_2$ under inert conditions and added as a solution in chlorobenzene to a solution of P(NDI2OD-T2). Accordingly, the resulting absorption spectrum (Figure S7, Supporting Information) followed the same trends as previously described for P(NDI2OD-T2) doped with CO_2-DMBI, with a suppression of the peak ≈700 nm and an increase in absorption ≈485 nm. Interestingly, this was only observed on heating, with little change observed at room temperature. This implies a dual role of the thermal activation step, which is necessary not only for the decarboxylation of dopant precursors, but also to overcome the activation energy related to the electron transfer. This is reminiscent of how reduction reactions with similar carbene dimers are typically conducted under elevated temperature to facilitate the electron transfer.[62]

HOMO levels of the active dopant species are of great importance, since they may reveal the limitations of the dopants with respect to host OSCs. Cyclic voltammetry (CV) was performed to achieve an estimation of energy levels, in this case by measuring the reduction potential of the corresponding cationic salt, due to the high reactivity of the neutral dimer species. The reduction potential of the dihexafluorophosphate salt $DMI_2(PF_6)_2$ dissolved in DMF has previously been reported as a two-electron reduction at −1.84 V against the ferrocene/ferrocenium couple (Fc/Fc^+), corresponding to an estimated DMI_2^{2+} LUMO at −2.96 eV.[63] Measuring the CV of $DMBI_2(PF_6)_2$ under equal conditions (Figure S8, Supporting Information) reveals a two-electron reduction peak at −1.33 V against Fc/Fc^+, indicating a lower $DMBI_2^{2+}$ LUMO at −3.47 eV. As these molecular orbitals correspond to the HOMOs of the neutral dimeric species, this may explain the lesser reducing effects of the CO_2-DMBI dopant compared to CO_2-DMI, as observed in the absorption spectra of doped OSCs. Either way, energy levels of both dopant dimers lie comfortably above the LUMOs of the doped OSCs, which range from −3.99 to −3.60 eV (Figure 3b), and thus should allow for efficient electron transfer.[64–67]

The energy levels obtained from CV data are in good agreement with density functional theory (DFT) calculations performed on the B3LYP/DZVP level. Calculations of $DMI_2(PF_6)_2$ and $DMBI_2(PF_6)_2$ complexes (whereby the HOMOs of the DMI_2 and $DMBI_2$ moieties become unoccupied as their electrons are transferred to the PF_6 counterparts) predict LUMO energy levels of the cationic dimers at −3.10 and −3.54 eV respectively (Figure S9a,b, Supporting Information), which lies within 0.15 eV of values obtained through CV. Calculations on isolated neutral dimers (in absence of PF_6^-) resulted in slightly deeper HOMO levels at −3.46 and −3.90 eV for DMI_2 and $DMBI_2$ respectively (Figure 3c; Figure S9c,d, Supporting Information). This reduces the energy offset with respect to OSC LUMOs, with the $DMBI_2$ HOMO equal to or even slightly below the LUMOs of the studied OSCs. We note, however, that doping may still occur, if there is sufficient interaction between the dopant molecule and a proximal OSC unit.[29,37] As we will discuss shortly, this is indeed the case for the dopants and OSCs of interest in this work. Meanwhile, the calculated HOMO levels of both carboxylates and carbenes are very deep (−5.72 eV and lower, Figure S10, Supporting Information), ruling out spontaneous electron transfer from these species to the OSCs.

Further closed-shell DFT calculations on complexes between active dopant dimers and host OSCs show that DMI_2 interacts strongly with each OSC (so that the frontier HOMO orbitals of dopant-host complexes have contributions from both moieties), resulting in partial charge transfer from the dimer to the P(NDI2OD-T2), PCBM, or O-IDTBR, corresponding to 0.67, 0.30, and 0.61 electrons respectively (Figure 3d; Figure S11, Supporting Information). Interactions between $DMBI_2$ and P(NDI2OD-T2) resulted in a slightly lower partial charge transfer of 0.47 electrons. The unequivocal tendency of DMI_2 and $DMBI_2$ to donate electrons to the host OSCs has been verified with calculations employing a number of other basis sets, as detailed in Table S1 (Supporting Information). These findings confirm that both dimerized molecules act as n-type dopants for the respective OSC systems. Open-shell DFT calculations provide further evidence for electron transfer, showing that integer charge transfer of one electron from DMI_2 to either of the OSCs is energetically favorable over partial charge transfer by 0.05 to 0.40 eV. Furthermore, spin density plots obtained with constrained DFT calculations (Figure S12, Supporting Information) show that the resulting unpaired electrons are delocalized on the dopant and host moieties.

In addition, the species formed through hybridization with DMI_2 are predicted to have HOMO values of −3.99, −3.79, and −3.89 eV for P(NDI2OD-T2), PCBM, and O-IDTBR respectively. As these values lie near the LUMO values of the pristine OSCs (Figure 3b), there is a possibility that the doping process may involve an additional charge transfer step between such charge transfer complexes and surrounding OSCs; this is particularly the case for DMI_2, as the HOMO of the $DMBI_2$/P(NDI2OD-T2) complex is predicted at a deeper −4.31 eV.

2.3. Organic Field-Effect Transistors

To evaluate the ability of the dopants to improve device performance past the limits of pristine OSCs, bottom-contact top-gate (BC-TG) OFETs were fabricated. P(NDI2OD-T2), PCBM, and

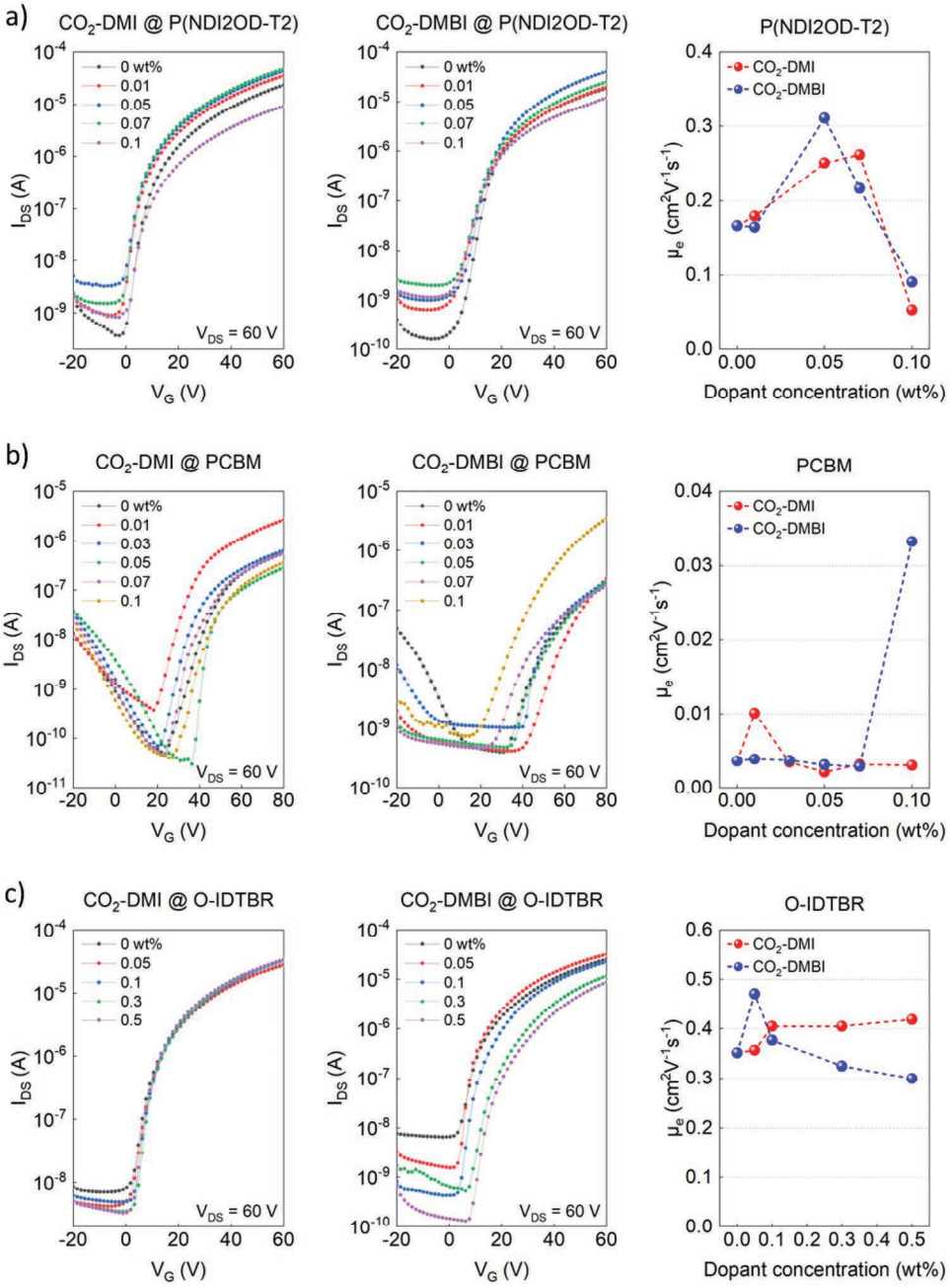

Figure 4. Representative transfer characteristics and electron mobilities of BC-TG OFETs containing a) P(NDI2OD-T2), b) PCBM, and c) O-IDTBR, doped with various concentrations of CO_2-DMI and CO_2-DMBI in the n-type OSC layer.

O-IDTBR were selected as the semiconductor layers to explore the versatility of the proposed dopants. The selected materials cover a range of well-known n-type materials, including polymers, small molecules, and fullerene and non-fullerene species, with a variety of LUMO levels. Dopants were activated prior to spin-coating by heating the pre-mixed solution in chlorobenzene to 80 °C for 1 h. **Figure 4** outlines representative transfer characteristics of devices made with each OSC and doped with various concentrations of either dopant as well as average mobility values at the respective doping levels. Furthermore, their output characteristics are plotted in Figures S13–S15 (Supporting Information) and all device parameters are outlined in Table S2 (Supporting Information).

P(NDI2OD-T2) devices doped with CO_2-DMI and CO_2-DMBI follow a similar pattern, where optimal doping concentrations were found at 0.07 and 0.05 wt.% respectively, followed by a decline in electron mobility at higher concentrations. At their optimal configuration, average electron mobility increased from 0.17 to 0.26 and 0.31 $cm^2\ V^{-1}\ s^{-1}$ respectively, with maximum values at 0.30 and 0.40 $cm^2\ V^{-1}\ s^{-1}$. As such, CO_2-DMBI was proven as a more efficient device dopant for P(NDI2OD-T2), approximately doubling electron mobility at optimal conditions.

The increase in device performance is also associated with a reduction of threshold voltage of ≈3.5 V in both cases, which is related to trap filling and increased electron density by the dopant addition. Upon 0.1 wt.% doping with either dopant, mobilities dropped below that of devices made with pristine P(NDI2OD-T2).

In PCBM devices, the two dopants seem to behave quite differently, most likely due to the ambipolarity of PCBM. Figure 4b shows the transfer characteristics from pristine and doped OFETs. In the case of CO_2-DMI it can be seen that the p-type character is present even at high dopant loadings, whereas in the case of CO_2-DMBI even small dopant addition results in suppression of the p-type character, allowing for higher n-type charge transport. At low dopant concentrations, CO_2-DMI outperforms its counterpart, with an average electron mobility value of 0.010 $cm^2\ V^{-1}\ s^{-1}$, almost three times as high as the pristine device at 0.0036 $cm^2\ V^{-1}\ s^{-1}$. Meanwhile, for CO_2-DMBI doped OFETs, mobility enhancement is achieved at higher dopant loadings. At 0.1 wt.%, the average device mobility was improved by almost one order of magnitude, reaching 0.033 $cm^2\ V^{-1}\ s^{-1}$, with a maximum value of 0.045 $cm^2\ V^{-1}\ s^{-1}$, and thus overall outperforming the CO_2-DMI. Further increasing the amount of dopant resulted in a reduction of performance.

Finally, devices made with O-IDTBR also demonstrated an increase in electron mobility upon doping. Doping with CO_2-DMI resulted in a subtle upswing in mobility upon 0.1 wt.% doping, and remained at a similar level also at 0.3 and 0.5 wt.%, reaching 0.42 $cm^2\ V^{-1}\ s^{-1}$, compared to the original 0.35 $cm^2\ V^{-1}\ s^{-1}$. Once again, CO_2-DMBI resulted in a greater improvement, reaching an average mobility of 0.47 $cm^2\ V^{-1}\ s^{-1}$ at 0.05 wt.%, but with a gradual decrease at higher concentrations. In both cases a reduction in threshold voltage was observed when doping with the optimum amount (Table S2, Supporting Information). Both CO_2-DMI and CO_2-DMBI have been demonstrated to successfully improve electron charge carrier mobility of OFETs upon optimization of dopant concentration.

2.4. Thin Film Morphology

The transistor results suggest that the electron affinity of the dopant is not the only factor influencing device properties, and changes in the active layer morphology may also play a role. Recent results have suggested that even at low doping concentrations, as in the current study, doping can fundamentally impact crystallization and orientation of the semiconductor.[5,57,68] To investigate the effect of doping on morphology, atomic force microscopy (AFM) was used to map the topography of spun-cast thin-films of each dopant/OSC system (**Figure 5**a; Figures S16–S18, Supporting Information). Here, we expanded our range of dopant concentrations, from low to very high (0, 0.05, 0.1, 1, and 10 wt.%).

Pristine P(NDI2OD-T2) exhibits a clearly fibrillar surface structure, with a root mean square (RMS) roughness of 2.12 nm, similar to what has previously been reported.[69,70] Within dopant concentrations that are relevant in a device context, i.e., 0.1 wt.% and below, no major changes could be seen to this pattern, with RMS values remaining similar to the pristine film. However, at 1 wt.%, the fibrillar structure appears to disintegrate; this is more prominent in the case of CO_2-DMI, while CO_2-DMBI retains a partly fibrillar surface structure. This is also reflected by the RMS, reported at 1.50 nm when doping with 1 wt.% CO_2-DMI, indicating a considerable flattening of the surface, compared to the lesser flattening of the CO_2-DMBI doped film with an RMS of 1.90 nm. At 10 wt.% dopant concentration, the fibrillar surface structure completely disintegrated in both films.

While AFM images of PCBM films did not exhibit any obvious surface patterns – showing featureless and smooth surfaces throughout – the surface topography of pristine O-IDTBR films appeared crystalline, with clear boundaries between adjacent sheet-like crystallites. This surface structure was maintained also after doping with up to 0.1 wt.% CO_2-DMI. At higher dopant concentrations significant change occurred, with the large platelets being replaced with a relatively featureless, smooth film (RMS = 0.295 nm, cf. ≥ 5.78 nm). In the case of CO_2-DMBI doping, the crystalline surface morphology was maintained up to 1 wt.% doping, followed by a similar morphological transition upon addition of 10 wt.% dopant (Figure S18, Supporting Information).

Another powerful tool to assess film morphology is X-ray diffraction (XRD).[71] To gain further insights into the morphological properties of doped OSCs, XRD measurements were conducted on films drop-cast onto silicon wafers (Figure 5b; Figure S19, Supporting Information). The diffraction pattern of pristine P(NDI2OD-T2) clearly displays the (200) and (300) lamellar peaks as well as the broad (010) π-stacking peak, in good agreement with literature, while the (100) peak is out of range.[72] The overall trend upon doping with CO_2-DMI is that the (200) *d*-spacing gradually decreases past 0.05 wt.% dopant concentration from ≈12.4 to ≈11.8 Å at 1 wt.%, with a significant drop to ≈10.3 Å at 10 wt.%. Meanwhile, lamellar spacing does not change upon doping with CO_2-DMBI until 10 wt.% concentration, resulting in a lesser drop from ≈12.4 to ≈11.1 Å. Furthermore, the lamellar peaks become more pronounced upon 10 wt.% doping, particularly in the case of CO_2-DMI. No clear trends are observed in the (010) *d*-spacing, which remains at ≈3.9 Å up until 1 wt.% dopant. At 10 wt.%, however, there is no longer any indication of ordered π-stacking as peaks disappear in favor of a broad, seemingly amorphous, peak. This is unsurprising, considering the complete disruption of fibrillar surface morphology at such concentrations, as observed with AFM. As such, we concluded that the dopant disturbs the morphology, albeit at loadings beyond the optimized OFET concentrations.

In the case of PCBM films, the pristine pattern has many features in common with crystalline PCBM as reported in literature, although slightly broadened and less defined than a fully crystalline species.[73] This indicates the presence of nanoscale crystallites in an amorphous environment. This pattern is largely maintained upon doping with 0.05 wt.% of either dopant, but starts to fade upon doping at 0.1 wt.%, particularly with CO_2-DMI. Upon doping with 1 wt.% CO_2-DMI, only two broad peaks remain, indicating an amorphous structure, while some crystalline features still remain upon doping with 1 wt.% CO_2-DMBI.[74] These features finally disappear at 10 wt.%. Likewise, pristine O-IDTBR exhibits crystalline features, again in

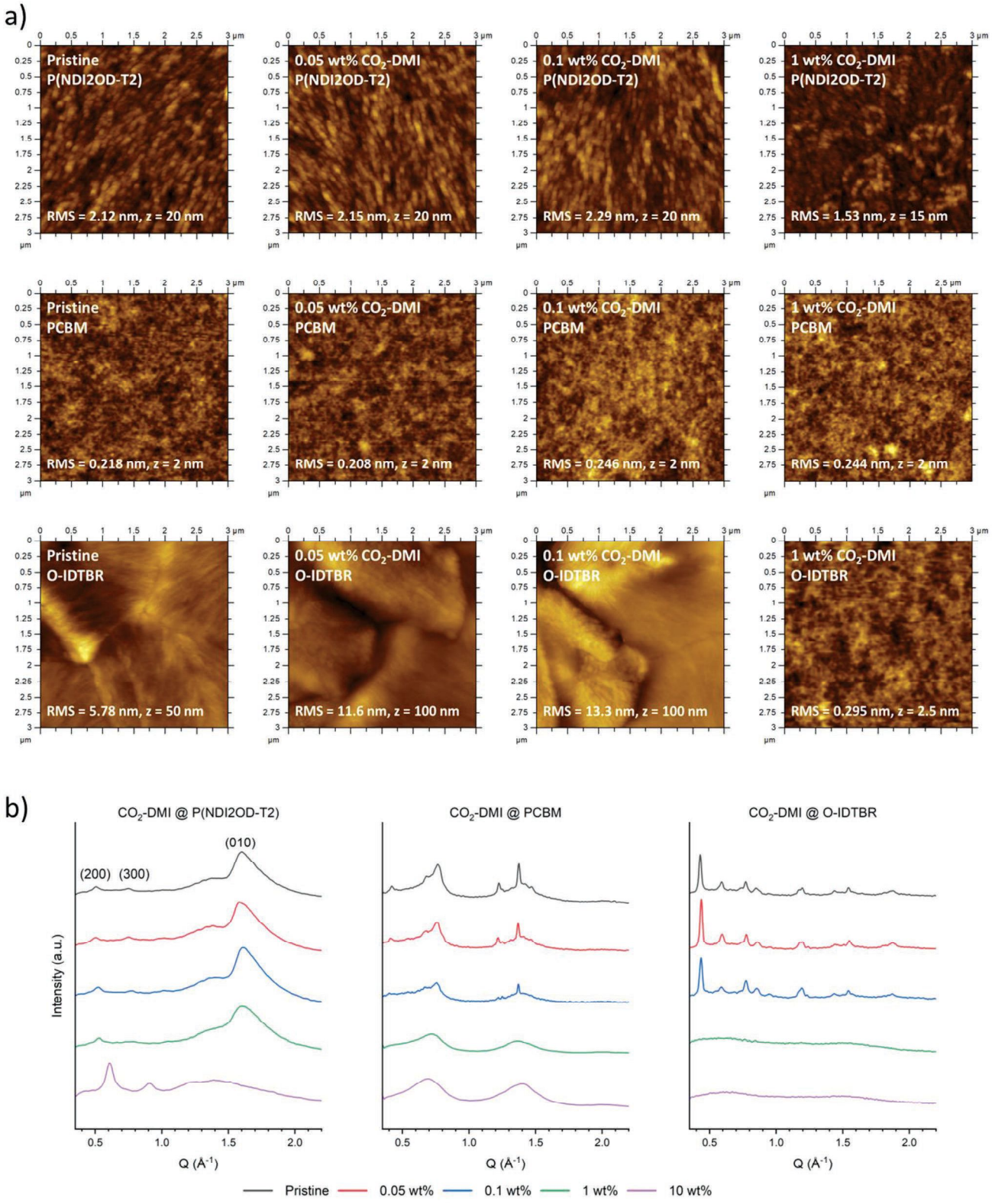

Figure 5. a) Topographical AFM images and b) XRD diffractograms of thin-films doped with CO_2-DMI.

agreement with previously reported diffractograms.[75] The crystalline structure is seemingly unaffected by addition of CO_2-DMI up to 0.1 wt.%, and of CO_2-DMBI up to 1 wt.%. At higher concentrations, all peaks disappear, indicating a complete disruption of the crystalline structure, in agreement with the AFM results.

3. Conclusion

In summary, CO_2-DMI and CO_2-DMBI have been demonstrated as effective and versatile dopants of n-type OSCs. While the dopant precursors remain stable and unreactive at room temperature – even under ambient conditions – UV–vis and EPR measurements of doped films and solutions indicate efficient electron transfer from the dopant to the host OSC upon in situ thermal activation in solution prior to film formation. Experimental and computational studies suggest the formation of dimeric species upon decarboxylation of the dopant precursors, which act as the active dopant species. Device data of doped OFETs employing P(NDI2OD-T2), PCBM, and O-IDTBR as the semiconductor layer shows an improvement of electron mobility for all materials with both dopants. Throughout, devices doped with CO_2-DMBI perform better than the corresponding devices doped with CO_2-DMI, with CO_2-DMBI doped PCBM devices exhibiting a 10-fold increase in electron mobility. AFM and XRD studies indicate that CO_2-DMBI has a lesser impact on the thin-film morphology of the investigated OSC systems, although the extent of these effects is not obvious at device-level dopant concentrations. Overall, this work highlights carboxylation as an effective design tool toward air-stable dopant precursors, which can be thermally activated in situ through thermal decarboxylation to enhance electron mobility of a wide range of n-type OSCs.

4. Experimental Section

A full description of experimental procedures is provided in the Supporting Information.

Supporting Information

Supporting Information is available from the Wiley Online Library or from the author.

Acknowledgements

The authors would like to thank the Engineering and Physics Science Research Council (EPSRC) (EP/V048686/1, EP/T028513/1, and EP/V057839/1), the Royal Society and Wolfson Foundation, and the King Abdullah University of Science and Technology (KAUST) Office of Sponsored Research (OSR) under Award No. OSR-2020-CRG8-4095 for financial support. F.A. acknowledges support from The Wilkinson Charitable Foundation. L.T. acknowledges support for the computational time granted from GRNET in the National HPC facility -ARIS – under project ATOMA. BJ thanks the Agence Nationale de la Recherche for the JCJC ANR grant "iPOD" (17-CE07-000101).

Conflict of Interest

The authors declare no conflict of interest.

Data Availability Statement

The data that support the findings of this study are available from the corresponding author upon reasonable request.

Keywords

electron transport enhancement, molecular doping, n-type dopants, organic field-effect transistors, organic semiconductors

Received: October 23, 2022
Revised: December 18, 2022
Published online: January 13, 2023

[1] G. Schweicher, G. Garbay, R. Jouclas, F. Vibert, F. Devaux, Y. H. Geerts, *Adv. Mater.* **2020**, *32*, 1905909.
[2] O. Inganäs, *Adv. Mater.* **2018**, *30*, 1800388.
[3] S.-J. Zou, Y. Shen, F.-M. Xie, J.-D. Chen, Y.-Q. Li, J.-X. Tang, *Mater. Chem. Front.* **2020**, *4*, 788.
[4] H. Bronstein, C. B. Nielsen, B. C. Schroeder, I. McCulloch, *Nat. Rev. Chem.* **2020**, *4*, 66.
[5] A. D. Scaccabarozzi, A. Basu, F. Aniés, J. Liu, O. Zapata-Arteaga, R. Warren, Y. Firdaus, M. I. Nugraha, Y. Lin, M. Campoy-Quiles, N. Koch, C. Müller, L. Tsetseris, M. Heeney, T. D. Anthopoulos, *Chem. Rev.* **2021**, *122*, 4420.
[6] K. Pei, *Surfaces and Interfaces* **2022**, *30*, 101887.
[7] K. Walzer, B. Maennig, M. Pfeiffer, K. Leo, *Chem. Rev.* **2007**, *107*, 1233.
[8] Y. Lin, M. I. Nugraha, Y. Firdaus, A. D. Scaccabarozzi, F. Aniés, A. Emwas, E. Yengel, X. Zheng, J. Liu, W. Wahyudi, E. Yarali, H. Faber, O. M. Bakr, L. Tsetseris, M. Heeney, T. D. Anthopoulos, *ACS Energy Lett.* **2020**, *5*, 3663.
[9] D. Li, F. Geng, T. Hao, Z. Chen, H. Wu, Z. Ma, Q. Xue, L. Lin, R. Huang, S. Leng, B. Hu, X. Liu, J. Wang, H. Zhu, M. Lv, L. Ding, M. Fahlman, Q. Bao, Y. Li, *Nano Energy* **2022**, *96*, 107133.
[10] Y. Lin, Y. Zhang, J. Zhang, M. Marcinskas, T. Malinauskas, A. Magomedov, M. I. Nugraha, D. Kaltsas, D. R. Naphade, G. T. Harrison, A. El-Labban, S. Barlow, S. De Wolf, E. Wang, I. McCulloch, L. Tsetseris, V. Getautis, S. R. Marder, T. D. Anthopoulos, *Adv. Energy Mater.* **2022**, *12*, 2202503.
[11] B. Lüssem, C. M. Keum, D. Kasemann, B. Naab, Z. Bao, K. Leo, *Chem. Rev.* **2016**, *116*, 13714.
[12] Y. Xu, H. Sun, A. Liu, H. H. Zhu, W. Li, Y. F. Lin, Y. Y. Noh, *Adv. Mater.* **2018**, *30*, 13.
[13] M. I. Nugraha, M. Gedda, Y. Firdaus, A. D. Scaccabarozzi, W. Zhang, S. Alshammari, F. Aniés, B. Adilbekova, A. Emwas, I. McCulloch, M. Heeney, L. Tsetseris, T. D. Anthopoulos, *Adv. Funct. Mater.* **2022**, *32*, 2202954.
[14] J. Panidi, A. F. Paterson, D. Khim, Z. Fei, Y. Han, L. Tsetseris, G. Vourlias, P. A. Patsalas, M. Heeney, T. D. Anthopoulos, *Adv. Sci.* **2018**, *5*, 1700290.
[15] A. F. Paterson, L. Tsetseris, R. Li, A. Basu, H. Faber, A. Emwas, J. Panidi, Z. Fei, M. R. Niazi, D. H. Anjum, M. Heeney, T. D. Anthopoulos, *Adv. Mater.* **2019**, *31*, 1900871.
[16] M. Pfeiffer, A. Beyer, T. Fritz, K. Leo, *Appl. Phys. Lett.* **1998**, *73*, 3202.
[17] A. F. Paterson, N. D. Treat, W. Zhang, Z. Fei, G. Wyatt-Moon, H. Faber, G. Vourlias, P. A. Patsalas, O. Solomeshch, N. Tessler, M. Heeney, T. D. Anthopoulos, *Adv. Mater.* **2016**, *28*, 7791.
[18] T. Mukhopadhyaya, T. D. Lee, C. Ganley, S. Tanwar, P. Raj, L. Li, Y. Song, P. Clancy, I. Barman, S. Thon, H. E. Katz, *Adv. Funct. Mater.* **2022**, *32*, 2208541.
[19] C. K. Chan, F. Amy, Q. Zhang, S. Barlow, S. Marder, A. Kahn, *Chem. Phys. Lett.* **2006**, *431*, 67.
[20] K. Harada, A. G. Werner, M. Pfeiffer, C. J. Bloom, C. M. Elliott, K. Leo, *Phys. Rev. Lett.* **2005**, *94*, 036601.
[21] T. Menke, D. Ray, J. Meiss, K. Leo, M. Riede, *Appl. Phys. Lett.* **2012**, *100*, 093304.
[22] P. Wei, J. H. Oh, G. Dong, Z. Bao, *J. Am. Chem. Soc.* **2010**, *132*, 8852.

[23] S. Jhulki, H.-I. Un, Y.-F. Ding, C. Risko, S. K. Mohapatra, J. Pei, S. Barlow, S. R. Marder, *Chem* **2021**, *7*, 1050.
[24] J. Han, A. Chiu, C. Ganley, P. McGuiggan, S. M. Thon, P. Clancy, H. E. Katz, *Angew. Chem., Int. Ed.* **2021**, *60*, 27212.
[25] X. Lin, B. Wegner, K. M. Lee, M. A. Fusella, F. Zhang, K. Moudgil, B. P. Rand, S. Barlow, S. R. Marder, N. Koch, A. Kahn, *Nat. Mater.* **2017**, *16*, 1209.
[26] H. Guo, C.-Y. Yang, X. Zhang, A. Motta, K. Feng, Y. Xia, Y. Shi, Z. Wu, K. Yang, J. Chen, Q. Liao, Y. Tang, H. Sun, H. Y. Woo, S. Fabiano, A. Facchetti, X. Guo, *Nature* **2021**, *599*, 67.
[27] S. Guo, S. B. Kim, S. K. Mohapatra, Y. Qi, T. Sajoto, A. Kahn, S. R. Marder, S. Barlow, *Adv. Mater.* **2012**, *24*, 699.
[28] B. D. Naab, S. Zhang, K. Vandewal, A. Salleo, S. Barlow, S. R. Marder, Z. Bao, *Adv. Mater.* **2014**, *26*, 4268.
[29] D. Yuan, D. Huang, C. Zhang, Y. Zou, C. Di, X. Zhu, D. Zhu, *ACS Appl. Mater. Interfaces* **2017**, *9*, 28795.
[30] C.-Y. Yang, Y.-F. Ding, D. Huang, J. Wang, Z.-F. Yao, C.-X. Huang, Y. Lu, H.-I. Un, F.-D. Zhuang, J.-H. Dou, C. Di, D. Zhu, J.-Y. Wang, T. Lei, J. Pei, *Nat. Commun.* **2020**, *11*, 3292.
[31] J. A. Murphy, *J. Org. Chem.* **2014**, *79*, 3731.
[32] E. Doni, J. A. Murphy, *Chem. Commun.* **2014**, *50*, 6073.
[33] J. Broggi, T. Terme, P. Vanelle, *Angew. Chemie Int Ed.* **2014**, *53*, 384.
[34] G. Tintori, P. Nabokoff, R. Buhaibeh, D. Bergé-Lefranc, S. Redon, J. Broggi, P. Vanelle, *Angew. Chem., Int. Ed.* **2018**, *57*, 3148.
[35] G. Tintori, A. Fall, N. Assani, Y. Zhao, D. Bergé-Lefranc, S. Redon, P. Vanelle, J. Broggi, *Org. Chem. Front.* **2021**, *8*, 1197.
[36] Y. Ding, C. Yang, C. Huang, Y. Lu, Z. Yao, C. Pan, J. Wang, J. Pei, *Angew. Chem., Int. Ed.* **2021**, *60*, 5816.
[37] I. Salzmann, G. Heimel, M. Oehzelt, S. Winkler, N. Koch, *Acc. Chem. Res.* **2016**, *49*, 370.
[38] A. Mityashin, Y. Olivier, T. Van Regemorter, C. Rolin, S. Verlaak, N. G. Martinelli, D. Beljonne, J. Cornil, J. Genoe, P. Heremans, *Adv. Mater.* **2012**, *24*, 1535.
[39] I. E. Jacobs, C. Cendra, T. F. Harrelson, Z. I. Bedolla Valdez, R. Faller, A. Salleo, A. J. Moulé, *Mater. Horiz.* **2018**, *5*, 655.
[40] B. D. Naab, S. Guo, S. Olthof, E. G. B. Evans, P. Wei, G. L. Millhauser, A. Kahn, S. Barlow, S. R. Marder, Z. Bao, *J. Am. Chem. Soc.* **2013**, *135*, 15018.
[41] Y. Zeng, W. Zheng, Y. Guo, G. Han, Y. Yi, *J. Mater. Chem. A* **2020**, *8*, 8323.
[42] J. Liu, B. Van der Zee, D. R. Villava, G. Ye, S. Kahmann, M. Kamperman, J. Dong, L. Qiu, G. Portale, M. A. Loi, J. C. Hummelen, R. C. Chiechi, D. Baran, L. J. A. Koster, *ACS Appl. Mater. Interfaces* **2021**, *13*, 29858.
[43] D. Trefz, A. Ruff, R. Tkachov, M. Wieland, M. Goll, A. Kiriy, S. Ludwigs, *J. Phys. Chem. C* **2015**, *119*, 22760.
[44] Y. Han, Z. Fei, Y.-H. Lin, J. Martin, F. Tuna, T. D. Anthopoulos, M. Heeney, *Npj Flex Electron* **2018**, *2*, 11.
[45] J. Liu, L. Qiu, R. Alessandri, X. Qiu, G. Portale, J. Dong, W. Talsma, G. Ye, A. A. Sengrian, P. C. T. Souza, M. A. Loi, R. C. Chiechi, S. J. Marrink, J. C. Hummelen, L. J. A. Koster, *Adv. Mater.* **2018**, *30*, 1704630.
[46] T. Matsuo, K. Kawabata, K. Takimiya, *Adv. Energy Sustain. Res.* **2021**, *2*, 2100084.
[47] S. S. Kim, S. Bae, W. H. Jo, *Chem. Commun.* **2015**, *51*, 17413.
[48] S. Rossbauer, C. Müller, T. D. Anthopoulos, *Adv. Funct. Mater.* **2014**, *24*, 7116.
[49] T. Biskup, *Appl. Phys. Lett.* **2021**, *119*, 010503.
[50] L. M. Cowen, P. A. Gilhooly-Finn, A. Giovannitti, G. LeCroy, H. Demetriou, W. Neal, Y. Dong, M. Westwood, S. Luong, O. Fenwick, A. Salleo, S. Heutz, C. B. Nielsen, B. C. Schroeder, *J. Mater. Chem. C* **2022**, *10*, 8955.
[51] V. Nesterov, D. Reiter, P. Bag, P. Frisch, R. Holzner, A. Porzelt, S. Inoue, *Chem. Rev.* **2018**, *118*, 9678.
[52] R. W. Alder, M. E. Blake, L. Chaker, J. N. Harvey, F. Paolini, J. Schütz, *Angew. Chem., Int. Ed.* **2004**, *43*, 5896.
[53] H. V. Huynh, in *Organomet. Chem. N-Heterocyclic Carbenes*, John Wiley & Sons, Ltd, Chichester, UK, **2017**, 17.
[54] J. Messelberger, M. Kumar, S. J. Goodner, D. Munz, *Org. Chem. Front.* **2021**, *8*, 6663.
[55] J. Messelberger, A. Grünwald, S. J. Goodner, F. Zeilinger, P. Pinter, M. E. Miehlich, F. W. Heinemann, M. M. Hansmann, D. Munz, *Chem. Sci.* **2020**, *11*, 4138.
[56] Y. Liu, P. E. Lindner, D. M. Lemal, *J. Am. Chem. Soc.* **1999**, *121*, 10626.
[57] J. Panidi, J. Kainth, A. F. Paterson, S. Wang, L. Tsetseris, A. Emwas, M. A. McLachlan, M. Heeney, T. D. Anthopoulos, *Adv. Funct. Mater.* **2019**, *29*, 1902784.
[58] S. Wang, H. Sun, U. Ail, M. Vagin, P. O. Å. Persson, J. W. Andreasen, W. Thiel, M. Berggren, X. Crispin, D. Fazzi, S. Fabiano, *Adv. Mater.* **2016**, *28*, 10764.
[59] D. C. Graham, K. J. Cavell, B. F. Yates, *J. Phys. Org. Chem.* **2005**, *18*, 298.
[60] P. I. Jolly, S. Zhou, D. W. Thomson, J. Garnier, J. A. Parkinson, T. Tuttle, J. A. Murphy, *Chem. Sci.* **2012**, *3*, 1675.
[61] Z. Dong, C. Pezzato, A. Sienkiewicz, R. Scopelliti, F. Fadaei-Tirani, K. Severin, *Chem. Sci.* **2020**, *11*, 7615.
[62] J. A. Murphy, T. A. Khan, S. Zhou, D. W. Thomson, M. Mahesh, *Angew. Chem., Int. Ed.* **2005**, *44*, 1356.
[63] Y. Zhao, M. Rollet, L. Charles, G. Canard, D. Gigmes, P. Vanelle, J. Broggi, *Angew. Chem., Int. Ed.* **2021**, *60*, 19389.
[64] K. Akaike, K. Kanai, H. Yoshida, J. Tsutsumi, T. Nishi, N. Sato, Y. Ouchi, K. Seki, *J. Appl. Phys.* **2008**, *104*, 023710.
[65] J. Bertrandie, J. Han, C. S. P. De Castro, E. Yengel, J. Gorenflot, T. Anthopoulos, F. Laquai, A. Sharma, D. Baran, *Adv. Mater.* **2022**, *34*, 2202575.
[66] S. Wang, H. Sun, T. Erdmann, G. Wang, D. Fazzi, U. Lappan, Y. Puttisong, Z. Chen, M. Berggren, X. Crispin, A. Kiriy, B. Voit, T. J. Marks, S. Fabiano, A. Facchetti, *Adv. Mater.* **2018**, *30*, 1801898.
[67] D. Mori, H. Benten, I. Okada, H. Ohkita, S. Ito, *Energy Environ. Sci.* **2014**, *7*, 2939.
[68] D. T. Duong, C. Wang, E. Antono, M. F. Toney, A. Salleo, *Org. Electron.* **2013**, *14*, 1330.
[69] L. Tang, B. Watts, L. Thomsen, C. R. McNeill, *Macromolecules* **2021**, *54*, 11134.
[70] M. M. Nahid, A. Welford, E. Gann, L. Thomsen, K. P. Sharma, C. R. McNeill, *Adv. Electron. Mater.* **2018**, *4*, 1700559.
[71] A. Mahmood, J. Wang, *Sol. RRL* **2020**, *4*, 2000337.
[72] D. Simatos, L. J. Spalek, U. Kraft, M. Nikolka, X. Jiao, C. R. McNeill, D. Venkateshvaran, H. Sirringhaus, *APL Mater.* **2021**, *9*, 041113.
[73] R. Mens, S. Chambon, S. Bertho, G. Reggers, B. Ruttens, J. D'Haen, J. Manca, R. Carleer, D. Vanderzande, P. Adriaensens, *Magn. Reson. Chem.* **2011**, *49*, 242.
[74] H. Nakayama, J. A. Schneider, M. Faust, H. Wang, J. Read de Alaniz, M. L. Chabinyc, *Mater. Chem. Front.* **2020**, *4*, 3616.
[75] S. Holliday, R. S. Ashraf, A. Wadsworth, D. Baran, S. A. Yousaf, C. B. Nielsen, C.-H. Tan, S. D. Dimitrov, Z. Shang, N. Gasparini, M. Alamoudi, F. Laquai, C. J. Brabec, A. Salleo, J. R. Durrant, I. McCulloch, *Nat. Commun.* **2016**, *7*, 11585.